

RSC Advances

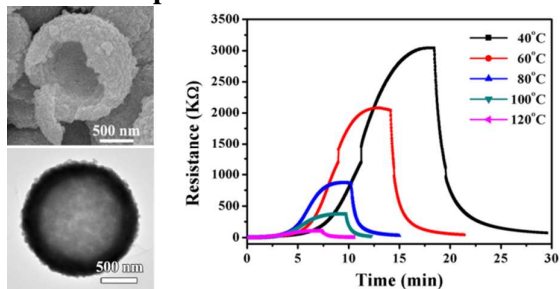


This is an *Accepted Manuscript*, which has been through the Royal Society of Chemistry peer review process and has been accepted for publication.

Accepted Manuscripts are published online shortly after acceptance, before technical editing, formatting and proof reading. Using this free service, authors can make their results available to the community, in citable form, before we publish the edited article. This *Accepted Manuscript* will be replaced by the edited, formatted and paginated article as soon as this is available.

You can find more information about *Accepted Manuscripts* in the [Information for Authors](#).

Please note that technical editing may introduce minor changes to the text and/or graphics, which may alter content. The journal's standard [Terms & Conditions](#) and the [Ethical guidelines](#) still apply. In no event shall the Royal Society of Chemistry be held responsible for any errors or omissions in this *Accepted Manuscript* or any consequences arising from the use of any information it contains.

Colour Graphic**Text:**

Hollow In₂O₃ microspheres were synthesized by a facile solvothermal method, and exhibited excellent sensing properties at low operating temperature.

Cite this: DOI: 10.1039/c0xx00000x

www.rsc.org/xxxxxx

ARTICLE TYPE

Facile Synthesis of Hollow In₂O₃ Microspheres and Their Gas Sensing Performances

Xiaolong Hu,^a Xin Zhou,^a Biao Wang,^b Peng Sun,^{*a} Xiaowei Li,^a Chen Wang,^a Jiangyang Liu,^a and Geyu Lu^{*a}

5 Received (in XXX, XXX) Xth XXXXXXXXXX 20XX, Accepted Xth XXXXXXXXXX 20XX

DOI: 10.1039/b000000x

Hollow In₂O₃ microspheres constructed by primary nanoparticles were successfully prepared by thermal treatment of the precursor, which was synthesized via a facile chemical solution route without any templates or surfactants. The images of field emission scanning electron microscopy (FESEM) and transmission electron microscopy (TEM) indicated that the sample was composed of a large number of hollow In₂O₃ microspheres with diameters of 1-2 μm. In addition, gas sensor based on the In₂O₃ hollow microspheres was fabricated and its gas sensing performances were investigated. It was found that sensors based on the as-prepared sample had a low operating temperature (80 °C), and exhibited high response, low detection limit and excellent selectivity to NO₂.

15 1. Introduction

In the past decade, the investigation of oxide semiconductor for gas sensing applications has become hot topic because of an increasing concern on the safety in environment and industrial activities.¹⁻³ For oxide semiconductor gas sensors, high sensitivity and excellent selectivity are the two most important parameters. Therefore, developing new strategies for increasing sensitivity and improving selectivity of sensors represent one of the major scientific challenges. A critical element in the pursuit of this quest is the discovery of efficient and cost-effective sensing materials. Due to well-defined interior voids, good surface permeability, low density, and high specific surface area, hollow structural sensing materials have attracted growing interest in recent years.⁴⁻⁹ Generally, the syntheses depend on complicated templating approaches,⁹⁻¹¹ in which hard or soft sacrificial templates are used to create a hollow structure. However, template contamination mostly decreases the activity of sensing materials and the synthetic procedure is tedious and high cost. In this regard, it is still highly desirable to develop facile, solution-based, and template free self-assembly methods for the preparation of hollow structures.

Indium oxide (In₂O₃) is a very important wide-band-gap (E_g = 3.6 eV) n-type semiconductor, well-known for its useful optoelectronic properties.¹²⁻¹⁴ In₂O₃ nanostructures can be synthesized via various methods and have found use in a variety of electronics applications.¹⁵⁻¹⁷ They are also of some interest as gas sensors, which have been found to be particularly sensitive to reducing gases^{18,19} such as ethanol and oxidizing gases^{20,21} such as nitrogen dioxide and ozone. Many studies have been conducted in order to improve the performance of gas sensors by reducing the size of In₂O₃ since Yamazoe demonstrated that a reduction in crystallite size could significantly enhance sensing performance.^{22, 23} However, the aggregation between the

nanoparticles will result in the degradation of the gas sensing properties. Recently, In₂O₃ with hollow structures have been demonstrated to be promising candidates for ultrasensitive sensors due to their unique structures, which are conducive to the diffusion and recognition of gas.²⁴ Herein, a one-step template-free solvothermal approach is reported for the synthesis of In₂O₃ hollow microspheres. When evaluated as the sensing material for gas sensor, the as-prepared In₂O₃ hollow microspheres manifested high response and excellent selectivity to NO₂ at a relatively low temperature (80 °C).

2. Experimental

2.1 Synthesis of In₂O₃ hollow microspheres

All the reagents in the experiment were purchased from Sinopharm Group Co. Ltd., and directly used without further purification. In a typical synthesis process, 0.26g of In(NO₃)₃·4.5H₂O and 0.5 g of urea were added to 40 mL absolute ethanol under vigorous stirring. After 40 min stirring, the mixture was transferred into a Teflon-lined stainless-steel autoclave and maintained at 160 °C for 12 h. After the autoclave was cooled to room temperature naturally, the precipitates were washed with deionized water and absolute ethanol for several times using centrifuge, and then dried at 80 °C. The obtained product was then calcined at 500 °C for 2 h in an air atmosphere using a muffle furnace.

2.2 Characterization

X-ray diffraction (XRD) patterns were recorded on a Rigaku D/Max-2550V X-ray diffractometer with Cu-Kα radiation (λ = 1.5406 Å) to analyze the crystal phases of the synthesized samples. The morphology of the product was examined by field emission scanning electron microscopy (FESEM, JEOL JSM-7500F

microscope operated at an acceleration voltage of 15 kV). Transmission electron microscopic (TEM), high-resolution transmission electron microscopic (HRTEM), and the corresponding selected-area electron diffraction (SAED) measurements were performed on a JEOL JEM-2100F transmission electron microscope with an acceleration voltage of 200 kV.

2.3. Fabrication and measurement of gas sensors

The as-prepared powder was mixed with deionized water to make a paste, which was then coated onto an alumina tube (4 mm in length, 1.2 mm in external diameter, and 0.8 mm in internal diameter, attached with a pair of gold electrodes) by a small brush to form a thick film. The thickness of sensing films was about 100 μm . After drying at room temperature for 30 min, the sensing devices were sintered at 400 $^{\circ}\text{C}$ for 2 h. A Ni-Cr heating wire was used to adjusting the operating temperature of the sensor. Finally, the sensor was constructed by connecting the corresponding junctions to the socket of sensor. A photo of the fabricated sensor was presented in Fig.1, and the corresponding parts of the sensor were marked in this figure. The measurement was processed by a static process in a test chamber which is made of glass. Environmental air was used as both a reference gas and a diluting gas to obtain desired concentrations of target gases. A given amount of the tested gas was injected into the test chamber, and the sensor was put into the chamber for the measurement of the sensing performance. When the response reached a constant value, the upper cover of the test chamber was removed and the sensor began to recover in air. The response of the sensor was defined as R_g/R_a for oxidizing gas and R_a/R_g for reduction gas, here R_g and R_a were the resistances of the sensor in the target gas and air, respectively. The response and recovery times are defined as the time taken by the sensor to achieve 90% of the total resistance change in the case of adsorption and desorption, respectively.

3. Results and discussion

3.1 Structural and morphological characteristics

The typical XRD pattern of the sample is shown in Fig. 2, from which all the diffraction peaks could be very well indexed to the cubic structure of In_2O_3 with the lattice parameter of

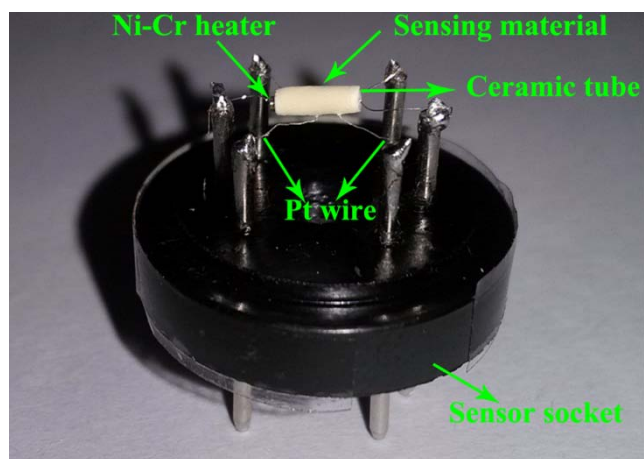


Fig. 1 Photograph of the fabricated sensor.

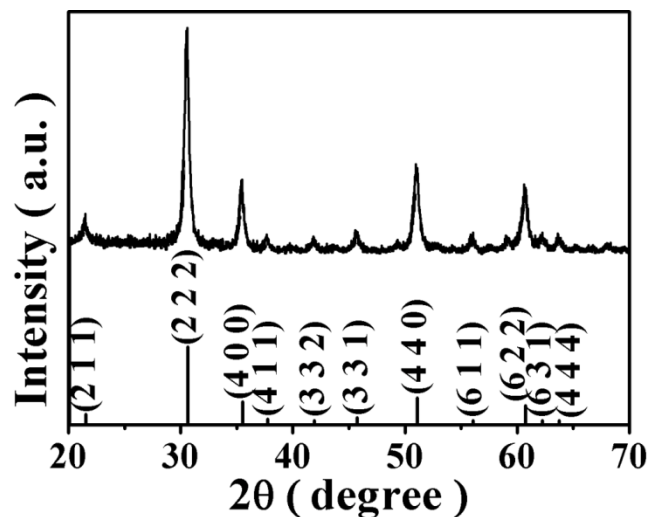


Fig. 2 XRD pattern of the In_2O_3 hollow microspheres and the standard XRD pattern of In_2O_3 (JCPDS No. 06-416).

$a=10.118 \text{ \AA}$, which were in good consistent with the standard file JCPDS No. 06-416 and the diffraction peaks in the XRD pattern are of high relative intensity, indicating the high crystallinity and high purity of the samples. The mean crystallite size of In_2O_3 was calculated to be around 16.6 nm using the Debye-Scherrer equation ($D=0.89\lambda/(\beta\cos\theta)$).

Field emission scanning electron microscopy (FESEM) observations were carried out to get insight into the morphology of In_2O_3 products. Fig. 3 presents a panoramic FESEM image of the In_2O_3 sample, which indicates that it was composed of spherical structures with sizes ranging from 1-2 μm . The hollow interior space can be clearly observed from the enlarged FESEM image of cracked microsphere (the inset of Fig.3). Furthermore, numerous primary particles with size of tens of nanometres piled up the hollow structure.

Further detailed morphological and structural analysis of the hollow microsphere was carried out using TEM, HRTEM and the corresponding SAED. The hollow nature of the In_2O_3 spheres could be further confirmed in the strong contrast between the dark edge and pale centre in the TEM image of an individual sphere (Fig. 4a), and it can be also observed that nanoparticles

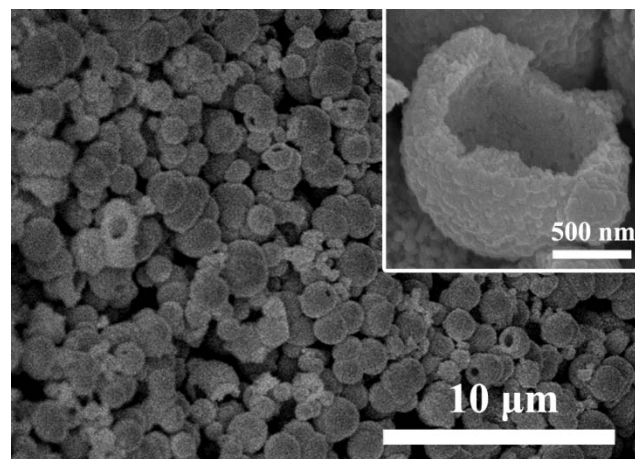


Fig. 3 A panoramic FESEM image of the In_2O_3 sample. The inset shows a cracked microsphere.

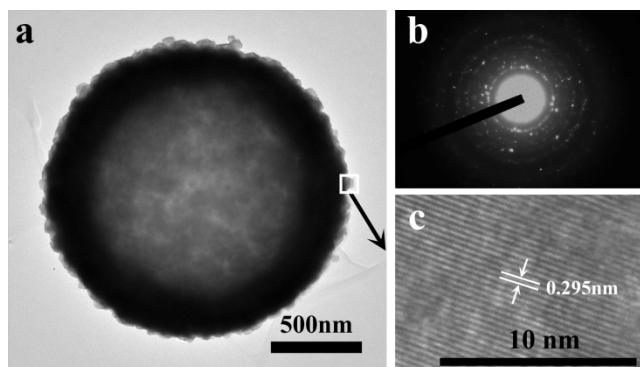


Fig. 4 (a) TEM image, (b) SEAD pattern and (c) HRTEM image of the calcined product (12h).

constructed the hollow spheres. The corresponding SAED pattern (Fig. 4b) demonstrated that the In_2O_3 hollow microspheres were polycrystalline structures in nature. Fig. 4c exhibits the HRTEM image obtained from the marked fringe of the In_2O_3 nanoparticles in Fig. 4a, from which the lattice fringes could be clearly observed and the distance of the adjacent lattice planes was measured to be 0.295 nm, corresponding to the (222) planes of In_2O_3 .

To understand the formation process of the hollow In_2O_3 microspheres, a series experiments were carried out at different reaction time (2 h, 8 h, and 12 h), and the evolutions of structure and morphologies of the calcined samples were examined by FESEM. As shown in Fig. 5, the growth process could be clearly divided into three stages. In the first stage (2 h, Fig.5a), solid spherical structures with very rough surface that composed of nanoparticles and nanosheets could be observed. With increasing reaction time (8h, Fig.5b), the surface of the spheres became less rough and the hollow characteristic emerged, which is the typical behaviour of ripening process. Upon prolonging reaction time to 12 h (Fig.5c), microspheres with hollow internal structure and rough surface were obtained. In general, the formation process could be summarized as a rapid self-assembly of nanosheets and nanoparticles into solid microspheres, followed by the component part that packed at the centre dissolved and transferred to the exterior. Based on the above analysis, Ostwald ripening process could be employed to explain the growth process.²⁵⁻²⁷

3.2 Gas sensing properties

The gas sensing performances of the sensor using hollow

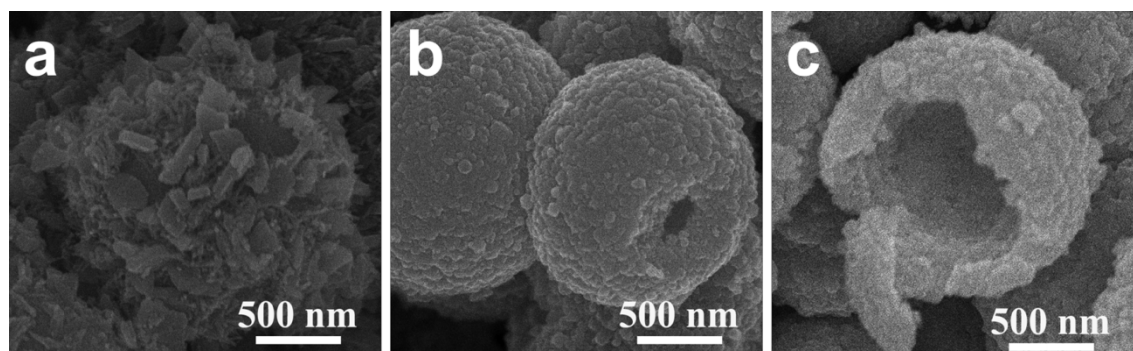


Fig. 5 SEM images of morphology evolution of hollow In_2O_3 microspheres prepared with different reaction time: (a) 2 h, (b) 8 h, (c) 12 h.

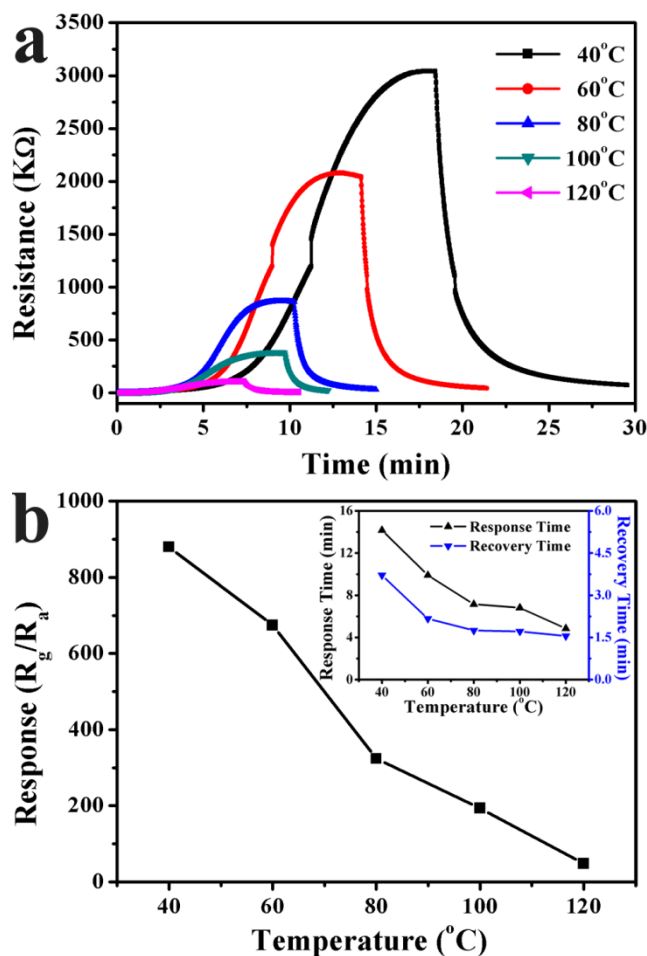


Fig. 6 (a) The dynamic response resistances of the fabricated sensor to 500ppb NO_2 at 40 °C, 60 °C, 80 °C, 100 °C and 120 °C. (b) The correlation of the response with the operation temperature. And (inset of b) the correlation of the response/recovery time with the operation temperature.

In_2O_3 microspheres were investigated. It is well known that the gas-sensing properties of a semiconductor gas sensor are significantly influenced by the operation temperature.²⁸ Because the adsorption/desorption processes and the competition for chemisorptions between NO_2 and atmospheric oxygen O_2 for the same active surface sites chemisorptions are both regulated by the temperature.²⁹ To find out the influence of the temperature to the

fabricated sensor, the response, response time and recovery time towards 500 ppb NO₂ were tested at varying operation temperature, as shown in Fig. 6. It is obvious that the response to NO₂ increased with the decrease of temperature, and the fabricated sensor exhibited excellent response to NO₂ at relatively low temperature. The response to 500 ppb NO₂ at 120 °C, 100 °C, 80 °C, 60 °C and 40 °C were about 47.5, 193.7, 323.5, 674.1 and 879.9, respectively. So the fabricated sensor could operate at relatively low temperature, which meant low power consumption and this was very important for a gas sensor to be put into use. Apart from response, response time and recovery time also need to be considered to comprehensive measure the gas sensing performance of a gas sensor. The correlation of the response time and recovery time with the operation temperature were presented in the inset of Fig.6b. As can be seen, the response time and recovery time also increased with the decrease of temperature. Roughly speaking, with the decrease of the temperature, the gas molecules became less and less active which led to the increase of the response time and recovery time. But the decrease of the temperature would also make the gas adsorption easier and the depth of gas diffusion deeper which will cause the high utilization rate of the sensing material, thus leading to higher response.³⁰⁻³⁴ Moreover, when the temperature was higher than 80 °C, the change of temperature had not obvious effects on the response time and recovery time. Therefore, although the response to 500 ppb NO₂ at 80 °C (323.5) was not the highest, considering response time and recovery time, 80 °C was chosen to be the optimal operation temperature of the fabricated sensor for NO₂ detection, which was employed to further investigate the sensing performances.

The relationship between response and NO₂ concentrations for the sensor at the operating temperature of 80 °C is displayed in Fig. 7a. From the curve, it is found that the responses of sensor increased with the gas concentration. The response to 50, 100, 200, 300, 400 and 500 ppb NO₂ were about 2.0, 3.1, 6.1, 39.1, 119.8 and 323.5, respectively. It is worth noting that the sensor showed an obvious response (2.0) even to NO₂ concentration as low as 50 ppb, which indicated that the sensor had a relatively low detection limit (shown in the inset of Fig. 7a). A comparison between the sensing performances of the sensor presented in this paper and literature reports is summarized in Table 1. It is noteworthy that the sensor fabricated in our work exhibits better sensing performance compared with those reported in the literature.

Except for response, response time and recovery time, selectivity is also an important parameter for gas sensor. Eight kinds of other gases were tested, including 100 ppm NO, NH₃, CO, methanol, ethanol and acetone, 50 ppm SO₂, and 500 ppb O₃. The test results are presented in Fig.7b. It is clear that the fabricated sensor exhibits the highest response to NO₂ among all these tested gases, and the response to 500 ppb NO₂ was at least dozens of times higher than the other tested gases at the optimum operation temperature (80 °C). The test results indicated that the gas sensor based on the hollow microspheres In₂O₃ possess an excellent selectivity to NO₂ against the other test gases.

The responses of the fabricated sensor to 500 ppb NO₂ under different relative humidity at 80 °C were also tested to find out the effect of the humidity on the response of the sensor. And the results were presented in Fig 7.c. The results indicated that the

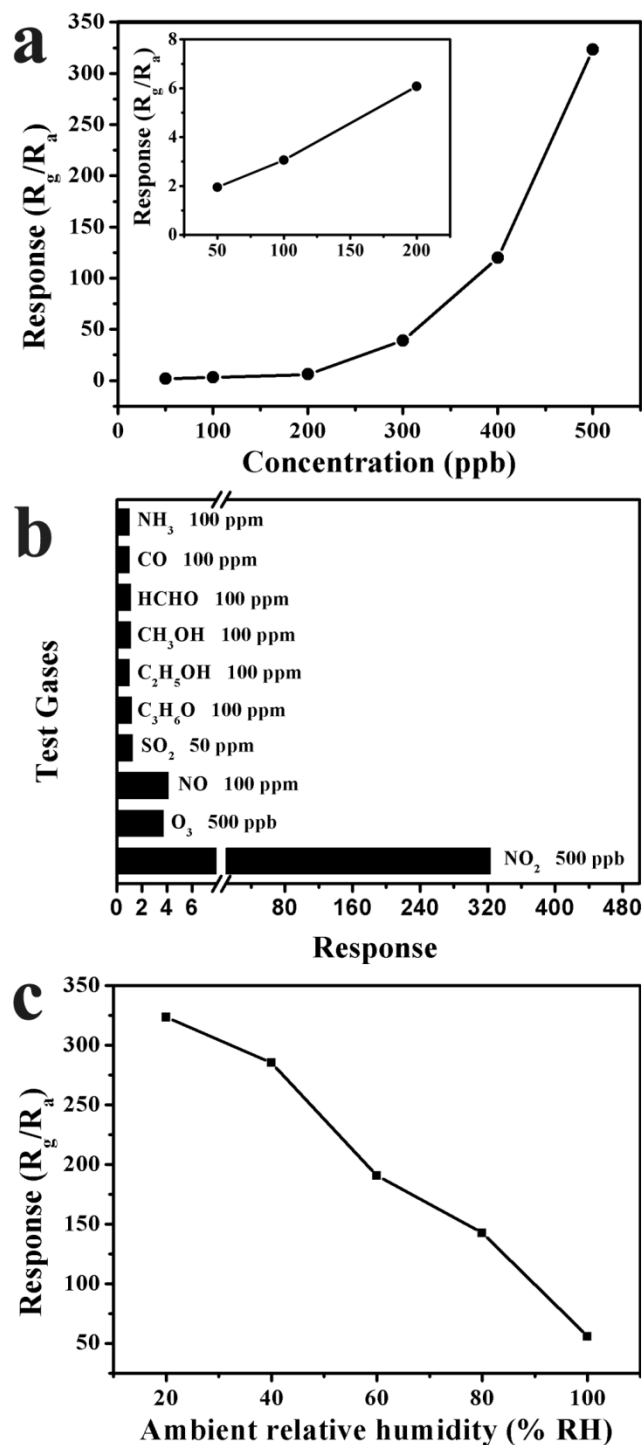


Fig. 7 (a) Response of the sensor versus NO₂ concentrations in the range of 50-500 ppb at 80 °C. (b) Response of the sensor to various test gases at 80 °C. (c) Response of the sensor to 500 ppb NO₂ under different relative humidity at 80 °C.

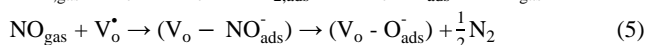
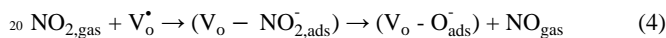
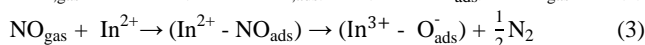
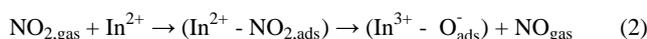
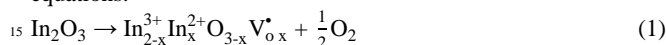
response decreased with the rise of relative humidity almost linearly. According to D. Vlachos et al.³⁵, the decrease might be caused by the active sites on the material surface were covered gradually by water molecules.

The most widely accept sensing mechanism of the sensor based on In₂O₃ to NO₂ gas can be stated as follow.³⁶⁻⁴² The electrical conductivity of In₂O₃ derives from electron transfer

Table 1 Comparison of gas-sensing characteristics of sensing material in present work and those reported in the literatures.

Material	NO ₂ concentration	Temperature (°C)	Sensor response	Reference
ordered mesoporous Fe-doped In ₂ O ₃	1ppm	150	71	43
mesoporous In ₂ O ₃ (UV light-enhanced)	5ppm	100	37.8	44
root slice-like In ₂ O ₃ microspheres	5ppm	250	1.5	45
Zn-In ₂ O ₃ flower-like structures	5ppm	300	~27.4	46
WO ₃ thin films	10ppm	150	57	47
WO ₃ hollow microspheres	1ppm	300	~54	48
hollow In ₂ O ₃ microspheres	500ppb	80	737.8	Present work

between In²⁺ and In³⁺, the formation of the In²⁺ occurring through oxygen deficiency (Eq.(1)). Anion vacancies V_o• and mainly partially reduced cations In²⁺ are the surface basic sites (S_b)_s for NO₂ chemisorption. And the formation of the chemisorption bond continued on the charge transfer from active sites (S_b)_s into an orbital of NO₂ causes a reduction in the strength of N-O bonds that makes the decomposition of the NO₂ molecules easier. Therefore, NO₂ molecules were reduced into NO or N₂ and the electronics of the In₂O₃ sensing materials were captured which led to the increase of the resistance of the sensor. The sensing mechanism could be summarized according to the following equations.



4. Conclusions

In summary, hollow In₂O₃ microspheres had been successfully synthesized by a simple solvothermal method and subsequent annealing process. FESEM and TEM images displayed that the microspheres were composed of nano-sized primary particles. Moreover, gas sensors based on the as-obtained hollow microspheres were fabricated and their sensing performances were investigated. It was found that the sensor exhibited high response, low detection limit and excellent selectivity to NO₂ at a low operating temperature (80°C).

Acknowledgment

This work is supported by the National Nature Science Foundation of China (Nos. 61374218, 61134010, and 61327804) and Program for Chang Jiang Scholars and Innovative Research Team in University (No. IRT13018). National High-Tech Research and Development Program of China (863 Program, No. 2013AA030902 and 2014AA06A505).

Notes and references

^a State Key Laboratory on Integrated Optoelectronics, College of Electronic Science and Engineering, Jilin University, Changchun, 130012, People's Republic of China.

⁴⁵ E-mail: spmaster2008@163.com, luyg@jlu.edu.cn;

Fax: +86 431 85167808; Tel: +86 431 85167808

^b Changchun Institute of Optics, Fine Mechanics and Physics, Chinese Academy Sciences, Changchun 130033, People's Republic of China.

1. A. Jerger, H. Kohler, F. Becker, H. B. Keller and R. Seifert, *Sensors and Actuators B-Chemical*, 2002, **81**, 301-307.
2. S. Ampuero and J. O. Bosset, *Sensors and Actuators B-Chemical*, 2003, **94**, 1-12.
3. N. Barsan, D. Koziej and U. Weimar, *Sensors and Actuators B-Chemical*, 2007, **121**, 18-35.
4. X. Zhou, C. Wang, W. Feng, P. Sun, X. Li and G. Lu, *Materials Letters*, 2014, **120**, 5-8.
5. Y. Cai, X. Li, Y. Liu, S. Du, P. Cheng, F. Liu, K. Shimanoe, N. Yamazoe and G. Lu, *Crystengcomm*, 2014, **16**, 6135-6140.
6. X. Li, W. Feng, Y. Xiao, P. Sun, X. Hu, K. Shimanoe, G. Lu and N. Yamazoe, *Rsc Advances*, 2014, **4**, 28005-28010.
7. P. Sun, X. Zhou, C. Wang, K. Shimanoe, G. Lu and N. Yamazoe, *Journal of Materials Chemistry A*, 2014, **2**, 1302-1308.
8. C. R. Michel, A. H. Martinez-Preciado, R. Parra, C. M. Aldao and M. A. Ponce, *Sensors and Actuators B-Chemical*, 2014, **202**, 1220-1228.
9. D. Han, P. Song, H. Zhang, Z. Yang and Q. Wang, *Materials Letters*, 2014, **124**, 93-96.
10. S.-J. Kim, I.-S. Hwang, C. W. Na, I.-D. Kim, Y. C. Kang and J.-H. Lee, *Journal of Materials Chemistry*, 2011, **21**, 18560-18567.
11. Y. Fan, S. Wang and Z. Sun, *Materials Chemistry and Physics*, 2012, **134**, 93-97.
12. R. A. Ismail, O. A. Abdulrazaq and K. Z. Yahya, *Surface Review and Letters*, 2005, **12**, 515-518.
13. Y. Li, W. Cai, G. Duan, F. Sun, B. Cao, F. Lu, Q. Fang and I. W. Boyd, *Applied Physics a-Materials Science & Processing*, 2005, **81**, 269-273.
14. A. M. E. Raj, K. C. Lalithambika, V. S. Vidhya, G. Rajagopal, A. Thayumanavan, M. Jayachandran and C. Sanjeeviraja, *Physica B-Condensed Matter*, 2008, **403**, 544-554.
15. D. E. Williams, *Sensors and Actuators B-Chemical*, 1999, **57**, 1-16.
16. B. Yagliglu, H. Y. Yeom, R. Beresford and D. C. Paine, *Applied Physics Letters*, 2006, **89**.
17. D. H. Zhang, C. Li, S. Han, X. L. Liu, T. Tang, W. Jin and C. W. Zhou, *Applied Physics Letters*, 2003, **82**, 112-114.
18. N. Du, H. Zhang, B. Chen, X. Ma, Z. Liu, J. Wu and D. Yang, *Advanced Materials*, 2007, **19**, 1641-+.
19. P. Song, D. Han, H. Zhang, J. Li, Z. Yang and Q. Wang, *Sensors and Actuators B-Chemical*, 2014, **196**, 434-439.
20. G. Korotcenkov, A. Cerneavski, V. Brinzari, A. Vasiliev, M. Ivanov, A. Cornet, J. Morante, A. Cabot and J. Arbiol, *Sensors and Actuators B-Chemical*, 2004, **99**, 297-303.

21. X. Xu, D. Wang, J. Liu, P. Sun, Y. Guan, H. Zhang, Y. Sun, F. Liu, X. Liang, Y. Gao and G. Lu, *Sensors and Actuators B-Chemical*, 2013, **185**, 32-38.
22. C. Xu, J. Tamaki, N. Miura and N. Yamazoe, *Sensors and Actuators B: Chemical*, 1991, **3**, 147-155.
23. N. Yamazoe, *Sensors and Actuators B: Chemical*, 1991, **5**, 7-19.
24. J.-H. Lee, *Sensors and Actuators B-Chemical*, 2009, **140**, 319-336.
25. X. Li, P. Sun, T. Yang, J. Zhao, Z. Wang, W. Wang, Y. Liu, G. Lu and Y. Du, *Crystengcomm*, 2013, **15**, 2949-2955.
26. Y. Qin, F. Zhang, Y. Chen, Y. Zhou, J. Li, A. Zhu, Y. Luo, Y. Tian and J. Yang, *Journal of Physical Chemistry C*, 2012, **116**, 11994-12000.
27. X. Chen, X. Jing, J. Wang, J. Liu, D. Song and L. Liu, *CrystEngComm*, 2013, **15**, 7243-7249.
28. V. R. Shinde, T. P. Gujar and C. D. Lokhande, *Sensors and Actuators B-Chemical*, 2007, **123**, 701-706.
29. X. Xu, P. Zhao, D. Wang, P. Sun, L. You, Y. Sun, X. Liang, F. Liu, H. Chen and G. Lu, *Sensors and Actuators B-Chemical*, 2013, **176**, 405-412.
30. N. Yamazoe, G. Sakai and K. Shimanoe, *Catalysis Surveys from Asia*, 2003, **7**, 63-75.
31. A.-M. Andringa, N. Vlietstra, E. C. Smits, M.-J. Spijkman, H. L. Gomes, J. H. Klootwijk, P. W. Blom and D. M. De Leeuw, *Sensors and Actuators B: Chemical*, 2012, **171**, 1172-1179.
32. N. Yamazoe and K. Shimanoe, *Sensors and Actuators B: Chemical*, 2008, **128**, 566-573.
33. N. Matsunaga, G. Sakai, K. Shimanoe and N. Yamazoe, *Sensors and Actuators B: Chemical*, 2003, **96**, 226-233.
34. G. Sakai, N. Matsunaga, K. Shimanoe and N. Yamazoe, *Sensors and Actuators B: Chemical*, 2001, **80**, 125-131.
35. D. Vlachos, P. Skafidas and J. Avaritsiotis, *Sensors and Actuators B: Chemical*, 1995, **25**, 491-494.
36. C. S. Rout, K. Ganesh, A. Govindaraj and C. N. R. Rao, *Applied Physics a-Materials Science & Processing*, 2006, **85**, 241-246.
37. L. Francioso, A. Forleo, S. Capone, M. Epifani, A. M. Taurino and P. Siciliano, *Sensors and Actuators B: Chemical*, 2006, **114**, 646-655.
38. M. Ivanovskaya, P. Bogdanov, G. Faglia and G. Sberveglieri, *Sensors and Actuators B: Chemical*, 2000, **68**, 344-350.
39. M. Ivanovskaya, A. Gurlo and P. Bogdanov, *Sensors and Actuators B: Chemical*, 2001, **77**, 264-267.
40. M. Epifani, J. D. Prades, E. Comini, E. Pellicer, M. Avella, P. Siciliano, G. Faglia, A. Cirera, R. Scotti and F. Morazzoni, *The Journal of Physical Chemistry C*, 2008, **112**, 19540-19546.
41. A.E. Solovjeva, V.A. Zhdanov, V.A. Markov, R.R. Shvangeradze, *Inorg. Mater.*, 1982, **18**, 825-828.
42. A. Gurlo, N. Barsan, M. Ivanovskaya, U. Weimar and W. Gopel, *Sensors and Actuators B: Chemical*, 1998, **47**, 92-99.
43. J. Zhao, T. Yang, Y. Liu, Z. Wang, X. Li, Y. Sun, Y. Du, Y. Li and G. Lu, *Sensors and Actuators B-Chemical*, 2014, **191**, 806-812.
44. T. Wagner, C.-D. Kohl, C. Malagu, N. Donato, M. Latino, G. Neri and M. Tiemann, *Sensors and Actuators B-Chemical*, 2013, **187**, 488-494.
45. Z. Cheng, L. Song, X. Ren, Q. Zheng and J. Xu, *Sensors and Actuators B-Chemical*, 2013, **176**, 258-263.
46. P. Li, H. Fan, Y. Cai and M. Xu, *Crystengcomm*, 2014, **16**, 2715-2722.
47. Z. Liu, T. Yamazaki, Y. Shen, T. Kikuta and N. Nakatani, *Sensors and Actuators B-Chemical*, 2007, **128**, 173-178.
48. C.-Y. Lee, S.-J. Kim, I.-S. Hwang and J.-H. Lee, *Sensors and Actuators B-Chemical*, 2009, **142**, 236-242.